J. of Thermal Science Vol.9, No.2

# Numerical Prediction of Turbulent Flow and Heat Transfer with Phase Change in Crystallizer of Inverse Casting

**Yanhui FENG Xinxin ZHANG Zhongbo XU Xinhua WANG**
University of Science & Technology Beijing, 100083 Beijing, China

A two-dimensional mathematical model has been undertaken to describe coupled liquid steel's turbulent flow and heat transfer with solidification in the crystallizer of inverse casting. The solid-liquid phase change phenomena have been modeled by using the continuum formulations and considering the mush zone as porous media. The turbulence flow has been accounted for, using a modified version of the low-Reynolds-number $k-\varepsilon$ turbulence model. A well-known numerical procedure, SIMPLE, has been used to solve the control equations. The effects of some main parameters on the solidification behavior have been studied, such as the casting speed, the thickness and the initial temperature of mother sheet, the superheat degree of liquid steel.

**Keywords: turbulent flow, heat transfer, phase change, inverse casting, continuum model**

## Introduction

Inverse casting is a technique for producing near-net-shape cast strips. The main idea of this technique is developed from a successful investigation[1], in which it has been proved that the inverse casting technique would be applicable to produce the steel strip with a thickness of 0.5~3 mm, with a good material property and with a lower energy consumption in contrast with conventional continuous casting process. The possibility to produce composite strips is also one of the most attractive prospects of this technique. Although a number of mathematical models of fluid flow and heat transfer for continuous caster/casting systems[2,5] have been developed, no study has been carried out for the inverse casting. The aim of the present study is to physical-mathematically model 2-D coupled turbulent flow and solidification phenomena in crystallizer of inverse casting. With computed flow patterns and solidification behaviors, the effects of some main parameters, e.g. the speed of mother sheet, have been studied.

## Physical-Mathematical Model

### Physical Model and Assumptions

Considering that the sheet's thickness is much smaller than its width, the crystallizor of inverse casting is simplified to a two-dimensional symmetrical system. The half of the crystallizor is schematically shown in Fig.1. The mother sheet with an initial thickness, $2l_{stripin}$, moves from bottom to top at a constant speed, $v_0$. The final sheet thickness, $2l_{stripout}$, is solved simultaneously with the velocity field and the temperature field. In order to keep the mass conservation, the supplementary liquid steel is continuously injected into the crystallizer from the inlet with a constant temperature, $T_{steelin}$, and a constant velocity, $u_{steelin}$, which is also one part of the

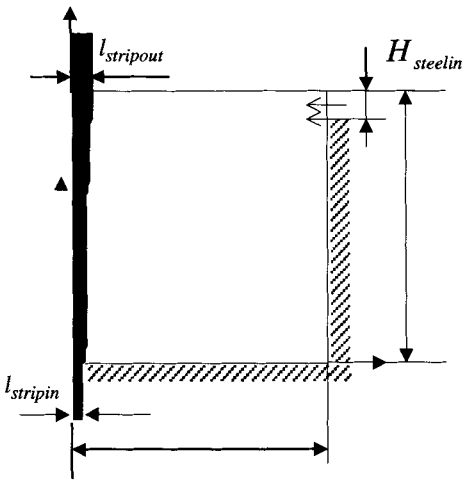


**Fig.1** Semi-crystallizor of inverse casting

Received 2000.

solutions. Assumptions invoked in the development of the mathematical model include:

(1) steady state with respect to a fixed coordinate system;
(2) incompressible and Newtonian turbulent flow in the liquid phase;
(3) local thermodynamic equilibrium during solidification;
(4) constant thermophysical properties of liquid and solid phases;
(5) the liquid steel region being viewed as a binary *Fe-C* solution;
(6) the latent heat of $\delta - \gamma$ transformation being neglected in comparison with the latent heat of fusion;
(7) the dendritic solidification being assumed and the pore formation being ignored;
(8) the action of mass transfer being ignored.

**Mathematical Formulations**

Forced convective flow produced by the movement of mother sheet, along with the buoyancy effects and the injection of supplementary liquid steel, makes the flow turbulent in the liquid region in the crystallizor. A modified form of the low-Reynolds number $\kappa$-$\varepsilon$ model of turbulence is employed. The governing conservation equations have been derived on the basis of continuum formulations for binary alloys, as originally developed by Bennon and Incropera[3].

The mixture phase velocity is designated as $\vec{v}$, which is defined as $\vec{v} = f_s\vec{v}_s + f_l\vec{v}_l$, where $\vec{v}_l$ and $\vec{v}_s$ are the vectors of the liquid phase velocity and of the solid phase velocity, respectively. The mass fractions of liquid $f_l$ and solid $f_s$ are both in function of temperature and concentration. Then, the continuity equation can be shown as

$$\nabla\cdot(\rho\vec{v}) = 0 \tag{1}$$

The $x$-components of the mixture phase velocity and of the solid velocity are designated respectively as $u$ and $u_s$. The x-momentum equation can be obtained as follows:

$$\nabla\cdot(\rho\vec{v}u) = \nabla\cdot(\mu_{eff}\nabla u) - \mu(u-u_s)/K_{px} - \partial p/\partial x + S_u \tag{2}$$

where $\mu_{eff} = \mu + \mu_t$ (turbulent viscosity $\mu_t = \rho f_\mu C_\mu \kappa^2/\varepsilon$) and the second term on the right-hand side accounts for the phase interaction forces in the mushy zone. When the mushy zone is modeled as a porous media, the Darcy's law can be applied. Darcy's law suggests that phase interaction forces are proportional to the superficial liquid velocity relative to the velocity of porous solid. $K_{px}$ represents the x-component of anisotropic permeability of the mushy zone and can be calculated by the Carman-Kozeny equation

$$K_{px} = f_l^3/[D_l(1-f_l)^2] \tag{3}$$

where the parameter $D_l$ depends on the morphology of the mushy zone. It can be determined by experimental expression $D_l = 180/d^2$ [5]. On account for the contribution of turbulence, the source term $S_u$ is defined as

$$S_u = \frac{\partial}{\partial x}(\mu_{eff}\frac{\partial u}{\partial x}) + \frac{\partial}{\partial x}(\mu_{eff}\frac{\partial v}{\partial x}) \tag{4}$$

While $v$ is designated as the $y$-components of the mixture phase velocity, $v_s$ is the solid velocity in the $y$ direction, $v_s$=$v_0$. The equation of $y$-momentum can be obtained as follows

$$\begin{aligned}\nabla\cdot(\rho\vec{v}v) = \nabla\cdot(\mu_{eff}\nabla v) - \mu(v-v_s)/K_{py}\\ -\partial p/\partial y + S_v\end{aligned} \tag{5}$$

where $K_{py}$ represents the y-component of anisotropic permeability of the mushy zone. An isotropic permeability in the mushy zone may be assumed, and hence $K_{px}$= $K_{py}$= $K_p$. The source term $S_v$ is defined as

$$\begin{aligned}S_v = \frac{\partial}{\partial x}(\mu_{eff}\frac{\partial u}{\partial y}) + \frac{\partial}{\partial x}(\mu_{eff}\frac{\partial v}{\partial y})\\ + \rho g\beta_T(h_s - h_{s,ref})/c_p\end{aligned} \tag{6}$$

The last source term is the thermal buoyancy force, obtained using Boussinesq approximation[4], where $h_{s,ref}$ can be valued by the solid enthalpy of injected liquid steel.

The mixture phase enthalpy is designated as $h$, which is defined as $h = f_s h_s + f_l h_l$, where $h_s$ and $h_l$ each represents the solid enthalpy and the liquid enthalpy. The energy equation can be expressed as

$$\nabla\cdot(\rho\vec{v}h) = \nabla\cdot[\Gamma_{eff}\nabla h] + S_h \tag{7}$$

where $\Gamma_{eff} = \mu_t/\mathrm{Pr}_t + \mu/\mathrm{Pr}$ ($\mathrm{Pr}_t$ is turbulent Prandtl number) and the source term $S_h$ is derived as follows:

$$S_h = \nabla\cdot[\Gamma_{eff}\nabla(h_s - h)] - \nabla\cdot[\rho(h_l - h)(\vec{v} - \vec{v}_s)] \quad (8)$$

The first source term represents the quasi-diffusion term and the second term represents the quasi-convective term, that is, the energy flux associated with relative phase motion. It's noted that the second term is only applied within the mush zone and holds a zero value in the solid and liquid regions.

In order to close above conservation equations, a supplementary relationship for phase mass fractions has to be determined. If $f_l$ and $f_s$ are both assumed as linear functions of temperature [4], we have

$$f_l = (T - T_{sol})/(T_{liq} - T_{sol}) \quad (9)$$

**Turbulence Modeling**

In this case, the low-Re $\kappa$-$\varepsilon$ model is more preferable than standard $\kappa$-$\varepsilon$ model since the solid-mushy-liquid interfaces are unknown and have to be derived as a part of the solution. A modified version of the low-Re $\kappa$-$\varepsilon$ model of Launder and Sharma[6] is employed to handle the turbulence effects.

For each of $\kappa$ and $\varepsilon$ equations, the solidification has been taken into account by incorporating a damping source term. As shown in velocity equations $u$ and $v$, the damping source terms here are related to the liquid fraction as

$$S_\kappa = -\mu\kappa / K_p \quad \text{and} \quad S_\varepsilon = -\mu\varepsilon / K_p \quad (10)$$

They both yield zero values for $\kappa$ and $\varepsilon$ in the solid region, vary with liquid fraction in the mushy region and take zero values in the liquid region. Hence, the equations for $\kappa$ and $\varepsilon$ can be written as follows:

$$\nabla\cdot(\rho\vec{v}\kappa) = \nabla\cdot[(\mu + \frac{\mu_t}{\sigma_\kappa})\nabla\kappa] - \mu\kappa/K_p + G_\kappa - \rho\varepsilon + D \quad (11)$$

$$\nabla\cdot(\rho\vec{v}\varepsilon) = \nabla\cdot[(\mu + \frac{\mu_t}{\sigma_\varepsilon})\nabla\varepsilon] - \mu\varepsilon/K_p + C_1 f_1 \frac{\varepsilon}{\kappa} G_\kappa - C_2 f_2 \rho \frac{\varepsilon^2}{\kappa} + E \quad (12)$$

where the term of generation of turbulent kinetic energy is defined as

$$G_\kappa = 2\mu_t[(\frac{\partial u}{\partial x})^2 + (\frac{\partial v}{\partial y})^2 + \mu_t(\frac{\partial u}{\partial y} + \frac{\partial v}{\partial x})^2] \quad (13)$$

The coefficients and other additional terms in $\kappa$ and $\varepsilon$ equations are summarized in Table 1.

**Dimensionless Parameters, Boundary Conditions and Numerical Method**

In order to obtain the dimensionless expressions of the eqs. (1)、(2)、(5)、(7)、(11)ad (12), the following dimensionless variables are adopted:

$$X = x/H, \quad Y = y/H, \quad U_k = u_k/v_0,$$
$$V_k = v_k/v_0, \quad h_k^* = h_k/h_f^0, \quad \kappa^* = \kappa/v_0^2,$$
$$\varepsilon^* = \varepsilon H/v_0^2, \quad \mu_t^* = \mu_t/\mu, \quad P = p/(\rho v_0^2)$$

Reynolds number $\mathrm{Re} = \rho v_0 H/\mu$,

Grashof number $Gr_T = \rho^2 g\beta_T h_f^0 H^3/(c_p\mu^2)$, and

Prandtl number $\mathrm{Pr} = \mu c_p/\lambda$.

Where the subscripts $k = l, s$. The variable without subscript is of mixture.

The boundary conditions are as follows:

1) Entry of mother sheet ($0 < X \le l_{stripin}/H, Y = 0$):

$$U = 0, V = 1, h^* = c_p T_{stripin}/h_f^0, \kappa^* = 0, \varepsilon^* = 0$$

2) Bottom solid wall ($l_{stripin}/H < X < L/H, Y = 0$):

$$U = 0, V = 0, \partial h^*/\partial Y = 0, \kappa^* = 0, \varepsilon^* = 0$$

3) Exit of final sheet ($0 < X \le l_{stripout}/H$, $Y = 1$):

- the solid region ($T \le T_{sol}$):

$$U = 0, \quad V = 1, \quad \partial h^*/\partial Y = 0, \quad \kappa^* = 0 \quad \varepsilon^* = 0$$

- the mushy region ($T_{sol} < T < T_{liq}$):

$$\frac{\partial U}{\partial Y} = \frac{\partial V}{\partial Y} = \frac{\partial h^*}{\partial Y} = \frac{\partial \kappa^*}{\partial Y} = \frac{\partial \varepsilon^*}{\partial Y} = 0$$

4) Upper free liquid surface ($\frac{l_{stripout}}{H} < X < 1, Y = 1$):

$$\partial U/\partial Y = 0, \quad V = 0, \quad \frac{\partial h^*}{\partial Y} = \frac{\partial \kappa^*}{\partial Y} = \frac{\partial \varepsilon^*}{\partial Y} = 0$$

5) Symmetrical axis ($X = 0$, $0 \le Y \le 1$):

$$U = 0, V = 1, \partial h^*/\partial X = 0, \kappa^* = 0, \varepsilon^* = 0$$

**Table 1** Coefficients and Empirical Constants Used for the Low-Re Number Model of Launder-Sharma

| Parameters | Expression | Parameters | Expression |
|---|---|---|---|
| $D$ | $2\mu\frac{\partial(\sqrt{\kappa})}{\partial x_i}\frac{\partial(\sqrt{\kappa})}{\partial x_i}$ | $E$ | $2\frac{\mu\mu_t}{\rho}\frac{\partial^2 u_i}{\partial x_j\partial x_k}\frac{\partial^2 u_i}{\partial x_j\partial x_k}$ |
| $f_1$ | 1.0 | $f_2$ | $1.0-0.3\exp[-(\rho\kappa^2/\mu\varepsilon)^2]$ |
| $f_\mu$ | $\exp[-3.4/(1+\frac{\rho\kappa^2}{\mu\varepsilon}/50)^2]$ | $C_\mu$ | 0.09 |
| $C_1$ | 1.44 | $C_2$ | 1.92 |
| $\sigma_\kappa$ | 1.0 | $\sigma_\varepsilon$ | 1.3 |

6) Inlet of liquid steel ( $X=\frac{L}{H}, \left(1-\frac{H_{steelin}}{H}\right)\le Y\le 1$):

$$U=U_{steelin},\quad V=0,\quad h^*=c_pT_{steelin}/h_f^0+1.0,$$
$$\kappa^*=0.01U_{steelin}^2,\quad \varepsilon^*=\kappa^{*1.5}/H_{steelin}$$

7) Right side solid wall ( $X=\frac{L}{H}, 0\le Y<\left(1-\frac{H_{steeln}}{H}\right)$):

$$U=0,\quad V=0,\quad \partial h^*/\partial X=0,\quad \kappa^*=0,\quad \varepsilon^*=0$$

where $U_{steelin}$ can be obtained based on an inlet-outlet mass balance in crystallizor:

$$U_{steelin}=\left(\int_0^{l_{stripout}}Vdx-\int_0^{l_{stripin}}Vdx\right)/H_{steelin}$$

The SIMPLE series algorithm[7] is applied. The criteria to terminate iterations are as follows: (1) the algebraic sum of residues generated by the continuity equation for internal nodes satisfies $R_{sum}<10^{-8}$; the maximum of all nodal residues satisfies $R_{max}<10^{-8}$; (3) the enthalpy change during two immediate iterations satisfies the following inequality

$$Max\left|\left(H_i^{n+1}-H_i^n\right)/H_i^n\right|\le 10^{-3}.$$

## Simulation Results and Discussion

The basic parameters of a typical inverse casting and its crystallizor, employed by the model developed above, are listed in Table 2.

The velocity distribution and the streamlines in the liquid region are shown in figure 2. The mother sheet's movement, from bottom to top, and the impact action of supplementary liquid steel, result to form two reverse recirculations. The upper one is clockwise while the lower one is anti-clockwise. The depths of both recirculating zones depend on casting speed, liquid steel inlet height and shape of crystallizer.

**Table 2** Basic Parameters of Crystallizer

| Nomenclature | Symbol/ Unit | Value |
|---|---|---|
| Crystallizer width | $2L$/m | 1.0 |
| Crystallizer height | $H$/m | 0.95 |
| Initial thickness of mother sheet | $2l_{stripin}$/m | 0.002 |
| Height of liquid steel inlet | $H_{steelin}$/m | 0.095 |
| Speed of mother sheet | $v_0$/(m/min) | 28.5 |
| Temperature of injected liquid steel | $T_{steelin}$/°C | 1550 |
| Initial temperature of mother sheet | $T_{stripin}$/°C | 20 |
| Density | $\rho$/(kg/m$^3$) | 7020 |
| Dynamic viscosity | $\mu$/(Pa s) | $6.2\times10^{-3}$ |
| Specific heat | $c_p$/(J/kg K) | 680 |
| Thermal conductivity | $\lambda$/(W/m K) | 34.3 |
| Critical liquidus temperature | $T_{liq}$/°C | 1530 |
| Critical solidus temperature | $T_{sol}$/°C | 1495 |
| Latent heat | $h_f^0$/(J/kg) | $2.7\times10^5$ |
| Thermal expansion coefficient | $\beta_T$/(1/K) | $10^{-4}$ |

The temperature contours near the mother sheet surface are shown in figure 3, in which two continuous blackened curves represent the position of the solid-mush interface $X_{solidus}$ and the mush-liquid interface $X_{liquidus}$. The variation of $X_{solidus}$ shows that the liquid steel near the mother sheet first solidifies, then some solidified steel melts. The final thickness of frozen shell is of 5.93mm, 6 times as thick as the mother sheet. That is coincident with the experimental results [1].

### Effects of Casting Speed

By numerical simulation according to various casting speeds, we have found that there exits a lower limit value for $v_0$, namely 16.286m/min, as shown in figure 4. The mother sheet will melt down if it moves with a speed below this value.

### Effects of Initial Thickness of Mother Sheet

The thickness of frozen shell and of final sheet varying with initial thickness of mother sheet is shown in figure 5. The mother sheet will melt down if $l_{stripin}$ is less than 0.0015m.

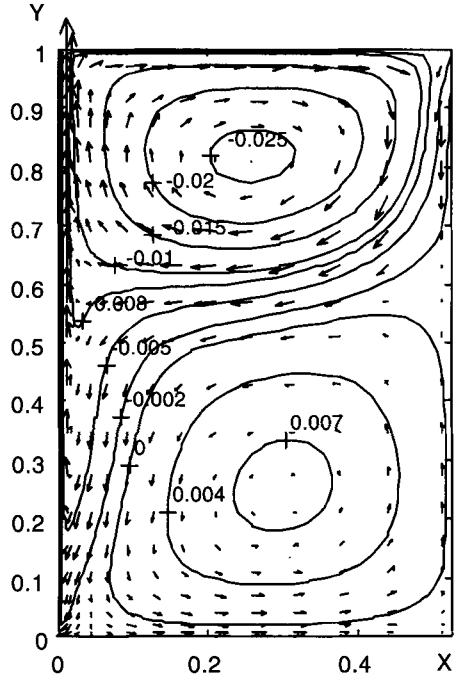


**Fig.2** Velocity distribution and streamlines in liquid steel phase with $v_0 = 28.5m/\min$ and $h_{steelin}$=0.1 H

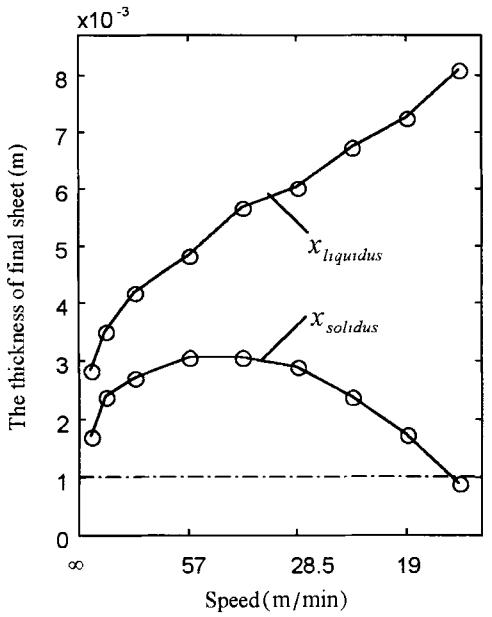


**Fig.4** Change of thickness of final sheet with different casting speeds

### Effects of Initial Temperature of Mother Sheet and Injected Liquid Steel

It's expected that both $x_{solidus}$ and $x_{liquidus}$ get smaller when initial temperature of mother sheet, $T_{stripin}$, or temperature of injected liquid steel, $T_{steelin}$, is

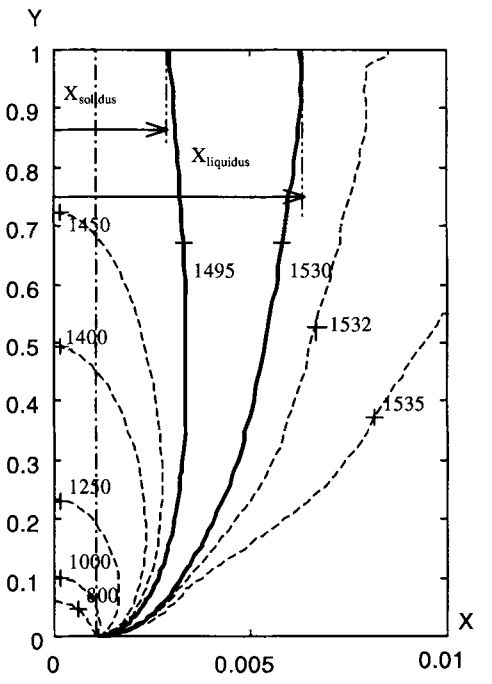


**Fig.3** Temperature distribution and phase interfaces with $v_0 = 28.5m/\min$ and $h_{steelin} = 0.1H$

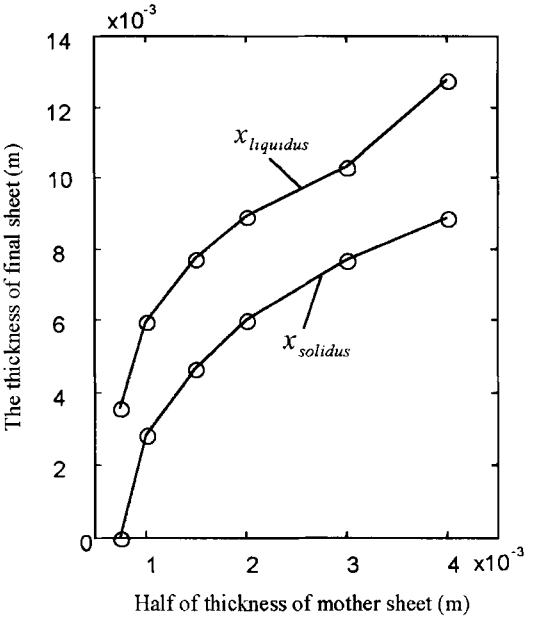


**Fig. 5** Change of thickness of final sheet with different initial thickness of mother sheet

increased, as shown in figure 6 and figure 7. For preventing the mother sheet from melting, the upper limits of $T_{stripin}$ and $T_{steelin}$ coming out of computation are $300^0$C and $1585^0$C, respectively.

## Conclusions

A two dimensional physical-mathematical model has been developed to describe liquid steel turbulent flow and heat transfer with solidification in inverse casting crystallizer. Solid-liquid phase change has been modeled by using the continuum formulation and considering mush zone as porous media. The turbulence phenomena in the crystallizer are simulated by using a modified version of the low-Reynolds-number $k-\varepsilon$ turbulence model. The velocity field and the temperature field in the crystallizer have been computed in order to study effects of casting speed, initial thickness of mother sheet, initial temperature of mother sheet and the injected liquid steel on the final sheet thickness.

## References

[1] Pleschiutchnigg et al., "Inversion Casting-a New Method for Producing Near-net-shape Cast Strips," Stahl und Eisen, **114**, No.2, pp.47-53, (1994).

[2] Shyy, W., Pang, Y., Hunter, G. B., Wel, D. Y., and Chen, M. H., "1992, Modeling of Turbulent Transport and Solidification during Continuous Ingot Casting," Int. J. Heat Mass Transfer, **35**, No.5, pp.1229-1245, (1992)

[3] Bennon, W. D. and Incropera, F. P., "A Continuum Model for Momentum, Meat and Species Transport in Binary Solid-liquid Phase Change Systems: I. Model Formulation," Int. J. Heat Mass Transfer, **30**, pp.2161-2170, (1987)

[4] Xinxin Zhang, Tong Lu, Yanhui Feng, Zhongbo Xu, Xinhua Wang, "Numerical Study of Fluid Flow and Heat Transfer in Crystallizer of Inverse Casting," Proceedings of 11th International Symposium on Transport Phenomena, Hsinchu, (1998)

[5] Aboutalebi, M. Reza, Hasan, M. and Guthrie, R. R. L., "Numerical Study of Coupled Turbulent Flow and Solidification for Steel Slab Casters," Numerical Heat Transfer. (A), **28**, No.3, pp.279-297, (1995)

[6] Tao, W. Q., "Numerical Heat Transfer," Publishing Corporation of Xi'an Jiaotong University, China, (1988).

[7] Patankar, S. V., "Numerical Heat transfer and Fluid flow," Hemiphere Publishing Corporation, New York, (1980)